Nanoscale

Accepted Manuscript

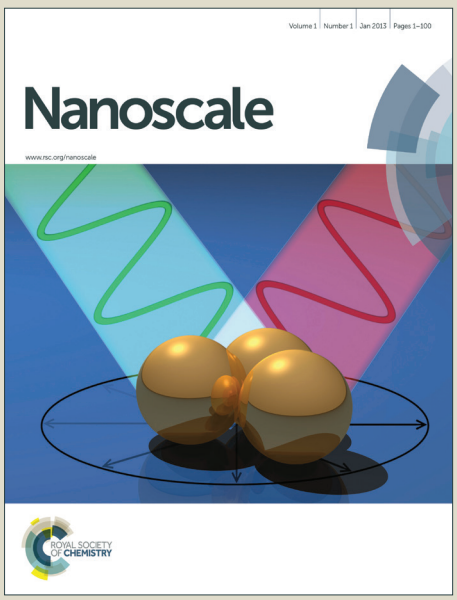

ROYAL SOCIETY OF CHEMISTRY

www.rsc.org/nanoscale

Nanoscale

PAPER

Easy conversion of protein-rich enoki mushroom biomass to nitrogen-doped carbon nanomaterial as a promising metal-free catalyst for oxygen reduction reaction

Received 00th January 20xx,
Accepted 00th January 20xx

DOI: 10.1039/x0xx00000x

www.rsc.org/

Chaozhong Guo[a,b]*, Wenli Liao[c], Zhongbin Li[c], Lingtao Sun[a], and Changguo Chen[b]*

In search of low-cost, highly active, and stable catalysts to replace the Pt-based catalysts for oxygen reduction reaction (ORR) has recently become a topic of interesting. Herein, we report a new strategy to design nitrogen-doped carbon nanomaterial for use as a metal-free ORR catalyst based on facile pyrolysis of protein-rich enoki mushroom (*flammulina velutipes*) biomass at 900 °C with carbon nanotube as a conductive agent and inserting matrix. We found that various forms of nitrogen (nitrile, pyrrolic and graphitic) were incorporated into the carbon molecular skeleton of the product, which exhibited more excellent ORR electrocatalytic activity and better durability in alkaline medium than those in acidic medium. Remarkably, the ORR half-wave potential measured on our material was around 0.81 V in alkaline medium, slightly lower than that on the commercial 20 wt.% Pt/C catalyst (0.86 V). Meanwhile, the ORR followed the desired 4-electron transfer mechanism involving the direct reduction pathway. The ORR performance was also markedly better than or at least comparable to the leading results in the literature based on biomass-derived carbon-based catalysts. Besides, we significantly proposed that the graphitic-nitrogen species that is most responsible for the ORR activity can function as the electrocatalytically active center for ORR, and the pyrrolic-nitrogen species can act as an effective promoter for ORR only. The results suggested a promising route based on economical and sustainable fungi biomass towards the large-scale production of valuable carbon nanomaterials as highly active and stable metal-free catalysts for ORR at alkaline conditions.

Introduction

Polarization loss owing to the oxygen reduction reaction (ORR) in fuel cells and metal-air batteries becomes one of the key factors that significantly influence the overall performance of these energy storage and conversion devices.[1,2] So far, platinum and its alloys have been considered as the best electrocatalysts for accelerating the ORR process.[3,4] In addition to prohibitively high cost, they suffer from drawbacks of poor stability, and susceptibility to crossover effect, which are becoming major hurdles for commercialization of these electrochemical power devices.[5] Generally, to reduce their cost and encourage widespread use, researchers have largely focused on replacing the expensive Pt-based catalyst with a lower-cost alternative for catalysis of the ORR.[6] Great efforts have been undertaken to the search for Pt-free catalysts, which has led to the discoveries of promising alternatives, containing non-precious metal catalysts (NPMCs),[7] nanostructured transition-metal oxides,[8,9] and nitrogen-doped carbon materials (NDCMs).[10-13] It is more interesting that nitrogen-doped carbon nanotubes (N-CNTs) as a significant class of NDCMs show great potential because of their high ORR electrocatalytic activity, excellent stability, and environmental friendliness.[14-16] At present, although the nature of the catalytically active sites for ORR in NDCMs still remains a controversial issue, there is no doubt that the ORR activity of NDCMs strongly depends on the selection of nitrogen precursors used and the utilization of advanced synthesis methods.[17] Lin, et al. powerfully confirmed that the rational selection of a N source is an effective way to enhance the ORR activity of NDCMs, and the nature of nitrogen functionalities are greatly affected by the structure of nitrogen precursors.[18]

However, the produced NDCMs using a great number of organic systems as N sources exhibit reasonable ORR activity, but their syntheses commonly need complex procedures and/or complicated chemicals.[5,15] For this purpose, the development of a facile method to synthesize highly active and stable NDCMs remains a challenge. One widely used strategy for synthesis of NDCMs is to use natural biomass as new N source of active site centers.[19,20] Several N-rich biomass previously reported in the literatures include soybean,[20] nori,[21] silk fibroin,[22] milk powder,[23] egg-white,[24] and hemoglobin.[25] Similar characteristics can be concluded, which are rich in amino acids and/or biologic proteins. We previously formed a series of NDCMs with good ORR activity and long durability via pyrolysis of

[a] Research Institute for New Materials Technology, Chongqing University of Arts and Sciences, Yongchuan, Chongqing 402160, China. E-mail:guochaozhong1987@163.com; cqchen@cqu.edu.cn
[b] School of Chemistry and Chemical Engineering, Chongqing University, Chongqing 400044, China.
[c] School of Materials and Chemical Engineering, Chongqing University of Arts and Sciences, Yongchuan, Chongqing 402160, China.

† Electronic Supplementary Information (ESI) available: Additional particle-size distribution data, BET surface area and pore size distributions, amperometric current-time curves, and comparison of ORR performance. See DOI: 10.1039/x0xx00000x

amino acid-rich and low-cost blood proteins from animals and carbon support nanomaterials,[26-28] and also explored their active site centers by carrying out rigorous design of experiments.[29] More recently, we developed another approach for green synthesis of NDCMs from the precursor of melamine, polyaniline, and CNTs.[30] Unfortunately, numerous researches have only investigated NDCMs synthesis and the ORR on NDCMs-catalyzed electrodes,[10,19–25] to the best of our knowledge, there is no report on the ORR of the NDCMs derived from various fungi.

Enoki mushrooms (*flammulinavelutipes*) are one of the most famous edible fungi around the world. They are abundantly and cheaply obtained; more than one million tons of enoki mushrooms are produced every year only in China, and they are sold for only ~2500 U.S. dollars per ton. The total content of bioprotein in dehydrated enoki mushroom is commonly between 30% and 40%. Herein, we report a facile "all-solid-state pyrolysis method" to efficiently synthesize N-doped carbon nanomaterial (N-C@CNT-900) as a metal-free catalyst for the ORR, which derives from bioprotein-rich enoki mushroom and carbon nanotubes. N-C@CNT-900 was carefully analyzed, and its ORR activity in alkaline and acidic media was examined in detail. We experimentally indicate that the pyrrolic-nitrogen species may be important to enhance the ORR activity only, and the graphitic-nitrogen species has played a significant role in maintaining the ORR activity of our material. Electrochemical results further suggest that our material has a critical function in the electrocatalysis of the ORR at alkaline and acidic conditions.

Experimental

Material synthesis

First, raw enoki mushroom (EM) supplied by the Food Testing Center of Chongqing Bureau of Quality and Technology Supervision was absolutely dried at 120 °C in a vacuum drying oven, and then ground in an agate mortar for about 2 h. 0.5 g of thoroughly dried and homogeneous EM powder as an only nitrogen source was adequately mixed with cheap carbon nanotubes (mass ratio of 2:1) by ball-milling for 5 h at 400 rpm. The produced precursor was subsequently pyrolyzed in a program-controlled tubular furnace under flowing N_2 atmosphere at 900 °C for 2 h to prepare a nitrogen-doped carbon nanomaterial, which was labelled as N-C@CNT-900. Notably, the length of used carbon nanotubes (CNTs, obtained from Beijing DK Nanotechnology Co. Ltd.) was 5~30 μm and its specific surface area was ~450 $m^2 g^{-1}$. The CNTs support was functioned as a conductive agent and inserting matrix to form catalytic sites in the pyrolysis process. The schematic illustration for synthesis of N-C@CNT-900 from EM biomass and CNTs support was shown in **Fig. 1**. As a control, the direct pyrolysis of dried EM powder at 900 °C for 2 h was performed for rapid synthesis of another kind of nitrogen-doped carbon material (N-C-900).

Physical characterizations

Powder X-ray diffraction (XRD) patterns of carbon materials were obtained on a Shimadzu XRD-6000 X-ray diffractometer using Cu Kα1 radiation (λ=1.5406 Å) at 4 ° min^{-1}. The Raman spectra were recorded with a Renishaw inVia unit using the Ar ion laser with an excitation wavelength of 514.5 nm. The size and surface morphology of carbon materials were imaged using electron microscopy facilities (Hitachi S-4700 high-resolution microscope operated at an acceleration voltage of 10 kV and JEOL FE-2010 high-resolution microscope operated at 200 kV). The particle size distribution of carbon materials was determined at a HORIBA Laser scatter particle-size distribution analyzer (Japan). X-ray photoelectron spectroscopy (XPS) analysis was investigated using a VG Scientific ESCALAB 220 iXL spectrometer with an Al Kα (hv=1486.69 eV) X-ray source. Nitrogen adsorption/desorption isotherms were measured at 77 K using Micromeritics ASAP 2010 Analyzer (USA) to obtain the Brunauer-Emmett-Teller (BET) surface area and pore size distribution.

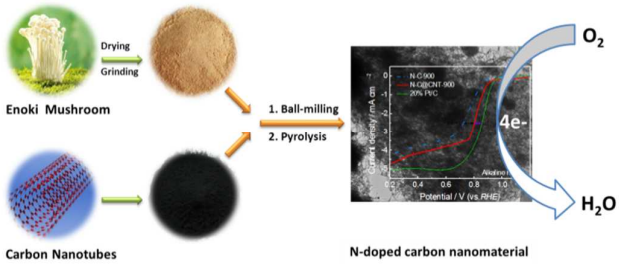

Fig. 1 Schematic illustration for easy preparation of N-C@CNT-900 from enoki mushroom biomass and CNTs support at controlled temperatures under N_2 protection.

Electrochemical measurements

The electrochemical properties of the products were tested in a three electrode system, and all electrochemical experiments were performed at room temperature on an Autolab workstation (μ Autolab III). A ring-shaped Pt wire and saturated calomel electrode (SCE) were used as the counter electrode and reference electrode, respectively. The electrolyte was 0.1 M KOH solution or 0.5 M H_2SO_4 solution which were purged by argon or oxygen for 30 min prior to the electrochemical test. A rotation disk electrode (RDE) with a glass carbon (GC, 4 mm diameter, 0.1256 cm^2 geometric area) electrode (Model 636, Princeton Applied Research) was employed as the working electrode. To prepare the modified-GC working electrode, the prepared carbon material was well-dispersed in the 0.5 wt.% Nafion/isopropanol solution. 5.0 μl of 10 mg ml^{-1} dispersion was transferred onto the GC disk surface and then dried at 80 °C. The mass loading was calculated to be around 0.40 mg cm^{-2}. A commercial Pt/C catalyst (20 wt.% Pt, E-ETK) on the GC electrode was prepared in the same way, but its mass loading was 0.32 mg cm^{-2}. All of electrode potentials in this work are quoted versus a reversible hydrogen electrode (RHE). All RDE and cyclic voltammetry (CV) experiments were performed over the potential range of 1.2 to 0.2 V at a scan rate of 5 mV s^{-1} in 0.1 M KOH solution, or the potential range of 1.1 to 0.1 V at a scan rate of 5 mV s^{-1} in 0.5 M H_2SO_4 solution. The stability of the catalyst was evaluated using an accelerated aging test (AAT). The AAT uses 2, 000 continuous potential cycles performed by cyclic scanning potential between 1.2 V to 0.1 V in different electrolytes. The

Koutecky-Levich (K-L) equation was used to analyse the number of electron transfer[31].

$$\frac{1}{j_d} = \frac{1}{j_k} + \frac{1}{0.62nFC_O D_O^{2/3} v^{-1/6} \omega^{1/2}}$$

where j_d and j_k are measured current density and kinetic-limiting current density respectively, F is the Faradaic constant; C_O is the O_2 saturation concentration in the electrolyte, D_O is the O_2 diffusion coefficient in the electrolyte, v is the kinetic viscosity of the solution, n is the number of electron transferred, ω is the electrode rotation rate, and 0.62 is a constant when the rotation rate is expressed in rpm.

Results and discussion

The wide-angle XRD patterns for EM biomass and two carbon materials are shown in **Fig. 2**a. The diffraction peaks of N-C-900, centered at 2θ = 25.0° and 43.5°, can be ascribed to the 002 and 101 lattice planes of a typical turbostratic carbon, respectively.[32] Compared with the diffraction peaks of carbon black (CB, Vulcan XC-72R),[29] the 002 peak of N-C-900 is negatively shifted and the full width-half maxima (FWHM) of the 002 peak is obviously increased, which are probably attributed to slight distortion in the crystalline regularity along the *a* or *b* direction and to vacancies caused by the introduction of nitrogen atoms into the sp^2 carbon lattice.[33] The N-C@CNT-900 has exhibited similar characteristics compared with the diffraction peaks of the CNTs support reported by Liao's group.[16] Notably, the 100 diffraction peak is observed at N-C@CNT-900 only, whereas the diffraction peaks of crystalline phases are not still observed. In contrast, the EM material obtained at 120 °C does not exhibit these highly desirable characteristics but does feature a weak amorphous-carbon peak at 20.8°, which may be due to its unfinished carbonization.[26] High-temperature pyrolysis of the EM material can effectively enrich the activated-carbon sources and largely increase the degree of graphitization.

We further performed the Raman spectroscopic analysis in order to study the defect sites and disordered structures. **Fig. 2**b depicts the Raman spectra of CB, CNTs and as-prepared samples. Each Raman spectrum was deconvoluted into two components by Lorentzian fitting, which exhibited the characteristic D and G peaks, respectively. The D band, located at ≈1350 cm^{-1}, is disorder induced, which corresponds to the sp^3 defect sites on the graphitic plane, mainly including vacancy and heteroatoms.[21] The G band, located at ≈1580 cm^{-1}, is commonly observed for all graphitic structures and attributed to the E_{2g} vibration mode present in the sp^2-bonded graphitic carbons, including C-C and C-N.[34] The intensity ratio of the D peak to the G peak, namely the I_D/I_G ratio, can provide the indication of the amount of structural defects and a quantitative measure of edge plane exposure. It is significantly found that the I_D/I_G ratio of N-C-900 (0.90) is larger than that of CB (0.88), and the I_D/I_G ratio of N-C@CNT-900 (0.58) is larger than that of CNTs (0.38), separately. Larger I_D/I_G ratio observed for N-doped samples can be a result of the structural defects and edge plane exposure caused by heterogeneous N atom incorporation into the graphene layers in both graphite and CNTs lattices.[29] Hence we can reasonably suppose that the CNTs have been effectively modified with N-rich products from the thermolysis of bioprotein inside EM biomass. It is additionally noted that the width at half maximum of the D peak (W_D) in all Raman spectra, corresponding to the amount of disordered carbon, is directly proportional to the I_D/I_G ratio of carbon materials. Therefore, the XRD and Raman spectroscopy data synergistically support this finding that the doping of N-heteroatom causes the increased defect sites in the carbon structure, and leads to a decrease in the graphitization of carbon materials prepared in this work.

The SEM image of N-C-900 (**Fig. 2**c) shows that this sample is mainly consisted of massive particles with different diameters, but many mini-sized particles are attached at their surface. The mean size of N-C-900 is ≈28.2 μm from the measurement of particle size distribution (Supporting information **Fig. 1**S). It must be pointed out that the irregular morphology of the particles is directly correlated to the degree of ball-milling. The SEM image of N-C@CNT-900 shows that it maintains similar morphology to the unpyrolyzed CNTs,[30] but some CNTs become larger in diameter and more inhomogeneous CNTs can be observed, as indicated in **Fig. 2**d. Besides, only a small number of carbon nanoparticles (CNP) are found in N-C@CNT-900, and their diameters are usually smaller compared to the N-C-900. The results demonstrate that addition of the CNTs into the precursor can hinder the agglomeration of carbon particles to a certain degree, and the CNTs has been modified with the decomposed products of EM, similar to our previous results.[26,35]

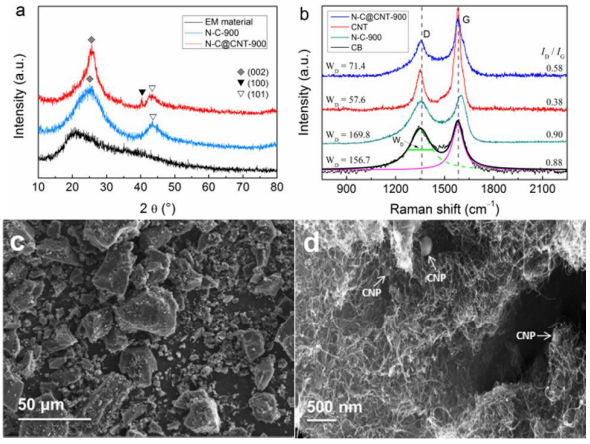

Fig.2. (a) The XRD patterns of EM material, N-C-900, and N-C@CNT-900. (b) The Raman spectra of carbon black, N-C-900, CNT material, and N-C@CNT-900. (c) The SEM image of N-C-900. (d) The SEM image of N-C@CNT-900.

The BET surface area of N-C-900 was measured to be 380.2 $m^2 g^{-1}$, and the averaged pore diameter was 2.1 nm (**Fig. 2**S). The BET surface area of N-C@CNT-900 was measured to be 305.3 $m^2 g^{-1}$, but the averaged pore diameter was 4.5 nm (**Fig. 3**S). Besides, the total pore volume of pores of N-C-900 (0.20 $m^3 g^{-1}$) was also smaller than that of N-C@CNT-900 (0.35 $m^3 g^{-1}$). These characteristics suggest that addition of CNTs support into the precursor can effectively increase the pore volume during pyrolysis, which may facilitate the mass transport process of O_2 molecule on N-C@CNT-900, and helps

to accelerate the ORR and enhance its ORR activity.[25] The BET surface area of N-C@CNT-900 is much smaller than that of prime CNTs (450 m^2 g^{-1}), which is similarly attributed to the modification of CNTs surface with N-containing products of EM decomposition.

Fig. 3 shows the HR-TEM images of two doped carbon materials. The structure and morphology of the samples are affected strongly by addition of the CNTs. The HR-TEM images of N-C-900 (**Fig. 3**b-c) demonstrate the amorphous carbon structure, and the lattice spacing is ~0.32 nm, which is almost consistent with the separation of (002) layers of hexagonal graphite.[32] Additionally, many dislocation defects can be observed in graphite layers due to the structure distortions caused by the incorporation of nitrogen atoms into graphite lattice in the carbon structure. This phenomenon can be equally observed in the HR-TEM images (**Fig. 3**d-f) of N-C@CNT-900. We can further confirm that N-doped carbon particles and N-doped CNTs co-exist in the prepared N-C@CNT-900 sample, and the CNTs have been modified with the decomposed products of EM, which results in the formation of defective and exposed edges because of the doping of nitrogen atoms.

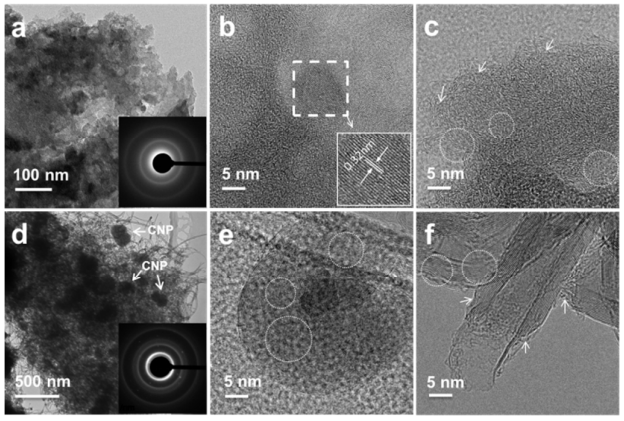

Fig. 3. The TEM images with electron diffractions of N-C-900 (a) and N-C@CNT-900 (d), and high-resolution TEM images of N-C-900 (b, c) and N-C@CNT-900 (e, f).

The XPS analysis of EM, N-C-900 and N-C@CNT-900 was performed to investigate their surface composition and chemical bonding, as shown in **Fig. 4**a. It is observed that C1s, N1s and O1s can be distinctly recognized from the XPS survey scan. The presence of N1s peak indicates that N atoms are successfully incorporated into the graphite structure of carbon materials, which is powerfully supported by their C1s XP spectra (**Fig. 4**b). The fitting C1s peaks located at 284.6, 285.9±0.1, 287.7±0.5, and 289.7±0.4 eV can be assigned to graphitic sp^2 carbon, amorphous carbon, sp^2 carbon atoms bonded to nitrogen, and sp^2 carbon atoms bonded to oxygen, respectively.[29,35,36] However, the occurrence of a peak located at 291.2 eV is owing to the π-π* shake up satellite in the C1s XP spectrum of N-C@CNT-900 only. We importantly found that the relative percentage of sp^2 C=N in N-C-900 (5.7%) was slightly lower than that in N-C@CNT-900 (6.3%), not only implying that the disruption of π conjugation on the outer layers of the carbon lattice due to the doping of N atoms, but also suggesting a higher content of nitrogen was doped into the internal carbon structure of N-C@CNT-900. The overall N content, which was determined *via* XPS analysis, was 5.27 % in EM but was only 3.43 %, and 3.20 % in N-C-900, and N-C@CNT-900, respectively (**Table 1**S). These ratios show that the pyrolysis process at 900 °C can highly affect the total N content of the doped carbon materials, resulting from the rapid evolution of nitrogen-based molecules inside EM biomass. However, a lower total N content in N-C@CNT-900 may be caused by the substantial addition of CNTs into the precursor during pyrolysis process and a higher total C content can be also observed at N-C@CNT-900 from **Fig. 4**a, whereas the amount of N-doping (namely N/C ratio) in N-C@CNT-900 can be not reduced in fact, resulting in the formation of more defect structures on the graphitic edge plane, which was supported by our previous results.[29]

The chemical status of N atom in the doped carbon materials was also probed by analysing the high-resolution N1s XPS peaks (**Fig. 4**c). The N1s XP spectra of EM can be deconvoluted into one peak only, which is assigned to Nitrile N from various amino acids and centered at the binding energy of ~399.6 eV. The N1s XP spectra of N-C-900 and N-C@CNT-900 can be deconvoluted into three peaks, which are attributed to nitrile N (~399.5 eV), graphitic N (~400.8 eV), and pyrrolic N (~400.2 eV) or oxidized N (~402.0 eV), respectively, in the carbon lattice.[29,36-38] It can be found that direct heat-treatment of EM at 900 °C has converted a large percentage (73.4%) of the nitrile N to graphitic and oxidized N species. Although a larger transformation of the nitrile N also occurs in the pyrolysis of EM and CNTs material, the formation of oxidized N species is absolutely hindered and the pyrrolic N species with a percentage of 33.3% is unexpectedly produced. Additionally, it is interesting that a lower percentage of nitrile N species has been preserved in N-C@CNT-900. Based on the results of HR-TEM, XPS and BET analysis, it can be reasonably concluded that the pyrrolic N species may be mainly formed by surface modification of the CNTs support.

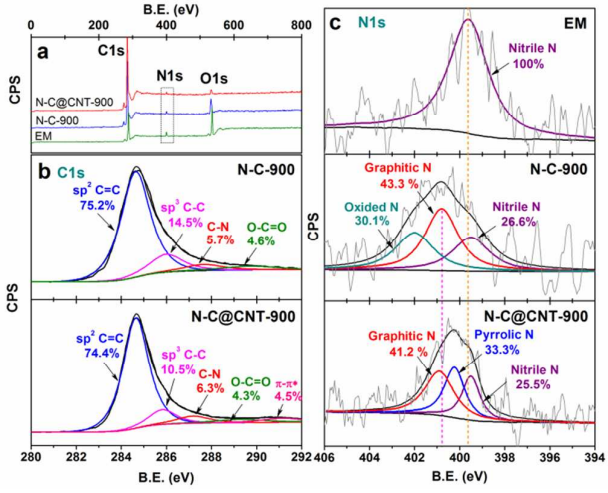

Fig. 4. (a) XP full-scan spectra of EM material, N-C-900, and N-C@CNT-900. (b) High-resolution C 1s XP narrow-scan spectra of N-C-900 and N-C@CNT-900. (c) High-resolution N 1s XP narrow-scan spectra of EM material, N-C-900, and N-C@CNT-900.

To assess the ORR electrocatalytic activity, our materials (N-C-900 and N-C@CNT-900) were first loaded (with the same mass loading) onto GC electrodes for CV in O_2 versus Ar-saturated alkaline electrolyte. **Fig. 5**a presents cyclic voltammograms (CVs) of N-C-900 and N-C@CNT-900 catalyzed electrodes in O_2 versus Ar-saturated 0.1 M KOH solution. Large difference between two carbon materials on the ORR activity can be obviously observed. The peak potentials of ORR are 0.718 V and 0.780 V (*vs.* RHE) for N-C-900 and N-C@CNT-900, respectively. Although the CVs of two materials have exhibited a visible ORR peak as expected, the ORR peak current density of N-C@CNT-900 is about twice larger than that of N-C-900, which was also confirmed by amperometric current-time (*i* - *t*) curves at 0.7 V vs. RHE (**Fig. 4**S). This difference powerfully demonstrates that N-C@CNT-900 possesses better ORR activity in alkaline medium. Besides, the CVs of N-C-900 and N-C@CNT-900 in an aqueous solution of 0.1 M KOH under Ar protection have displayed a virtually featureless curve (dash line in **Fig. 5**a). These results clearly indicated that significantly enhanced ORR activity was obtained by introduction of the CNTs into the precursor under the same heat-treatment condition, which was supported by our early reported results.[26]

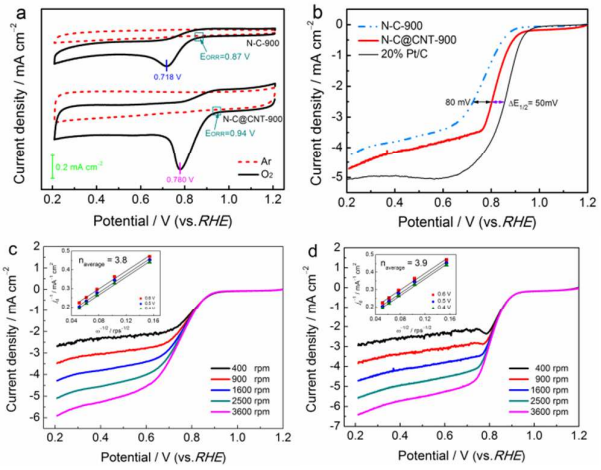

Fig. 5. (a) CVs of N-C-900 and N-C@CNT-900 in O_2 or Ar-saturated 0.1 M KOH electrolyte. (b) The ORR polarization curves of N-C-900, N-C@CNT-900 and 20 wt.% Pt/C catalyst in O_2-saturated 0.1 M KOH electrolyte at a rotation rate of 1600 rpm; the mass loading is 0.32 mg cm^{-2} for 20 wt.% Pt/C and is 0.40 mg cm^{-2} for the doped carbon catalysts. (c) The ORR polarization curves of N-C-900 in O_2-saturated 0.1 M KOH electrolyte at different rotation rates (400–3600 rpm). (d) The ORR polarization curves of N-C@CNT-900 in O_2-saturated 0.1 M KOH electrolyte at different rotation rates (400–3600 rpm); the insets represent the Koutecky-Levich plots of j_d^{-1} vs. $\omega^{-1/2}$ obtained from (c, d).

We used RDE measurements to further examine the ORR activity of prepared carbon materials and carbon-based platinum catalyst (E-ETK Co., denoted as 20 wt.% Pt/C) and reveal the kinetics of ORR in 0.1 M KOH electrolyte. The ORR polarization curves and corresponding catalytic activity data are displayed in **Fig. 5**b and **Table 1**S, respectively. The N-C@CNT-900-catalyzed electrode exhibits higher ORR electrocatalytic activity, but the N-C-900-catalyzed electrode also shows the activity for the ORR in terms of onset potential (E_{ORR}), half-wave potential ($E_{1/2}$), and limited current density (j_d). The half-wave potentials for ORR measured on a N-C@CNT-900-catalyzed electrode and a N-C-900-catalyzed electrode are 50 mV and 130 mV behind that on a state-of-the-art 20 wt.% Pt/C catalyst at a mass loading of 0.32 mg cm^{-2}, respectively. The ORR onset potential measured on a N-C@CNT-900-catalyzed electrode is about 0.94 V, lower than that on the 20 wt.% Pt/C catalyst (0.98 V). However, these results are comparable with those of the best N-doped carbon catalysts or noble-metal-free catalysts reported to date, in particular the catalysts derived from animal or plant biomass.[22–26] Hence it can be reasonably concluded that the N-C@CNT-900 is a very promising candidate for Pt-based catalysts.

The ORR polarization curves measured on N-C-900 and N-C@CNT-900 catalyzed electrodes in 0.1 M KOH electrolyte over a range of electrode rotation rates (400~3600 rpm) are indicated in **Fig. 5**c-d, respectively. As can be seen, an increase in the ORR current density with rotation rate was observed at two catalyzed electrodes. The linearity of the Koutecky-Levich (K-L) plots (insets of **Fig. 5**c-d) and near parallelism of the fitting lines suggested first-order dependence of the ORR kinetics and similar electron transfer numbers for ORR at different potentials. The numbers of electron transfer (n) were calculated to be ~3.8 and ~3.9 at 0.40–0.60 V for N-C-900 and N-C@CNT-900, respectively, based on the slopes of K-L plots. The average kinetic current densities at 0.4–0.6 V, obtained from the intercepts of K-L plots, were 12.38 mA cm^{-2}and 11.6 mA cm^{-2} for N-C@CNT-900 and N-C-900, separately. Our results indicated that the ORR on two carbon materials proceeded mainly with 4 e$^-$ reduction process ($O_2 + 2H_2O + 4e^- \rightarrow 4OH^-$), very similar to ORR catalysed by a state-of-the-art Pt/C catalyst measured in 0.1 M KOH electrolyte.[39]

We further measured the ORR electrocatalytic activity of N-C-900, N-C@CNT-900, and 20 wt.% Pt/C catalysts in O_2-saturated 0.5 M H_2SO_4 solution by CV and RDE techniques, as shown in **Fig. 6**. **Fig.6**a displays the ORR peak potentials of 0.445 V and 0.632 V for N-C-900 and N-C@CNT-900 in acidic electrolyte, respectively, but smaller than those in alkaline electrolyte. Surprisingly, no obvious ORR peak was observed at N-C-900-catalyzed electrode in acidic electrolyte, and its ORR peak current density was much lower than that of N-C@CNT-900-catalyzed electrode. An additional experiment amperometric i–t curves of N-C-900 and N-C@CNT-900 in O_2-saturated 0.5 M H_2SO_4 solution at 0.5 V vs. RHE was performed, as indicated in **Fig. 5**S. A larger ORR current density can be also observed at N-C@CNT-900-catalyzed electrode other than N-C-900-catalyzed electrode, which is in keeping with the electrochemical results tested in alkaline electrolyte (**Fig. 4**S).

The ORR polarization curves measured in 0.5 M H_2SO_4 electrolyte and corresponding catalytic activity data are displayed in **Fig. 6**b and **Table 1**S, respectively. In this electrolyte, the onset potential, half-wave potential, and limiting current density at +0.5 V of the N-C@CNT-900 electrode were 0.81 V, 0.60 V, and 2.85 mA cm^{-2}, respectively. All these values are between those of N-C-900 and 20 wt.% Pt/C catalyst. The half-wave potentials for ORR measured on a N-C@CNT-900-catalyzed electrode and a N-C-900-catalyzed electrode were 220 mV and 360 mV behind that on a state-of-the-art high-quality 20 wt.% Pt/C catalyst, respectively. It is very evident

that the N-C@CNT-900-catalyzed electrode shows much lower ORR activity in the acidic medium-comparable to the activity of 20 wt.% Pt/C -than in the alkaline medium. Remarkably, another difference between the performances in alkaline and acidic solutions here is an obvious plateau for the diffusion controlling kinetics on the polarization curves in the alkaline electrolyte, but almost no such plateau in the acidic medium. This phenomenon is related to the significantly improved kinetics of the ORR in alkaline electrolyte compare to in acidic electrolyte.

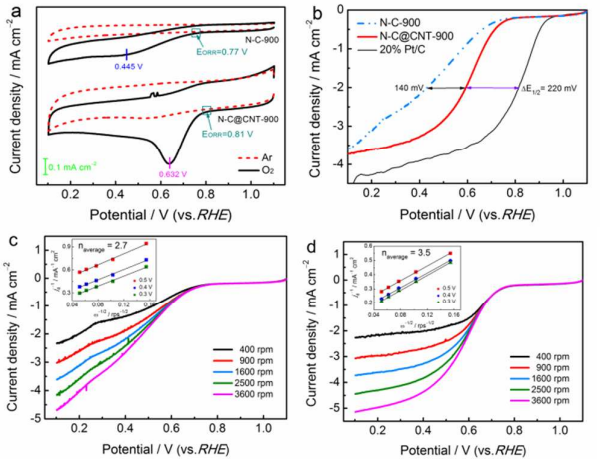

Fig. 6. (a) CVs of N-C-900 and N-C@CNT-900 in O_2 or Ar-saturated 0.5 M H_2SO_4 electrolyte. (b) The ORR polarization curves of N-C-900, N-C@CNT-900 and 20 wt.% Pt/C catalyst in O_2-saturated 0.5 M H_2SO_4 electrolyte at a rotation rate of 1600 rpm; the mass loading is 0.32 mg cm^{-2} for 20 wt.% Pt/C and is 0.4 mg cm^{-2} for the doped carbon catalyst. (c) The ORR polarization curves of N-C-900 in O_2-saturated 0.5 M H_2SO_4 electrolyte at different rotation rates (400–3600 rpm). (d) The ORR polarization curves of N-C@CNT-900 in O_2-saturated 0.5 M H_2SO_4 electrolyte at different rotation rates (400–3600 rpm). The insets represent the Koutecky-Levich plots of j_d^{-1} vs. $\omega^{-1/2}$ obtained from (c, d).

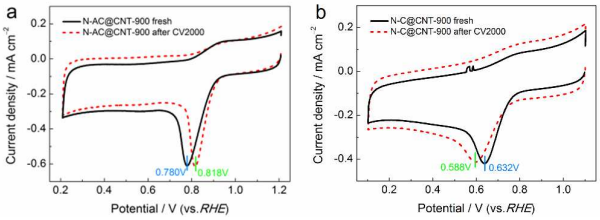

Fig. 7. LSVs of N-C-900 and N-C@CNT-900 in O_2-saturated 0.1 M KOH (a) and 0.5 M H_2SO_4 (b) electrolytes before and after N_2 cycling stability tests at a scan rate of 5 mV s^{-1}.

Fig. 6c-d shows that the current densities recorded at the N-C-900 and N-C@CNT-900 in acidic solution increase as the rotation speed increased (from 400 to 3600 rpm). The linearity and parallelism of K-L plots (insets) also indicate consistent electron transfer at different potentials and first-order reaction kinetics with respect to the concentration of dissolved oxygen. It was estimated from the K-L plots that the reaction electron numbers were ≈2.7 and 3.5 at 0.3–0.5 V for N-C-900 and N-C@CNT-900, respectively. Besides, the average kinetic current densities at 0.3–0.5 V, obtained from the intercepts of K-L plots, were 9.62 mA cm^{-2} and 5.15 mA cm^{-2} for N-C@CNT-900 and N-C-900, separately. These results suggest that the ORR catalyzed by N-C-900 can involve a mixture of two- and four-electron transfer pathways but is dominated by a two-electron transfer pathway to mainly produce HO_2^-. However, the ORR catalyzed by N-C@CNT-900 is dominated by a direct four-electron transfer pathway to produce H_2O, demonstrating relatively good activity of N-C@CNT-900 compared to N-C-900 in acidic electrolyte.

The stability for ORR in alkaline and acidic environments of N-C@CNT-900 is one of the most important factors to assess whether they can be applied to practical fuel cells. Thus, we here performed the continuous cycling stability tests in N_2-saturated 0.1 M KOH or 0.5 M H_2SO_4 electrolytes at a scan rate of 50 mV s^{-1}. The ORR activity of N-C@CNT-900 was further evaluated by linear sweep voltammograms (LSVs) under the same conditions as above experiments. No noticeable changes in onset potential and peak current density of the ORR were observed on the N-C@CNT-900-catalyzed electrode, and the ORR peak potential on this electrode were positively shifted by 38 mV in alkaline electrolyte, after CV cycling for 2, 000, indicating the extremely excellent stability of N-C@CNT-900, as shown in **Fig. 7**. However, the ORR peak potential on the N-C@CNT-900-catalyzed electrode was negatively shifted by 44 mV, and the onset potential and peak current density of the ORR have slightly decreased, after CV cycling for 2, 000, suggesting relatively poor stability of N-C@CNT-900 in acidic electrolyte comparing with in alkaline electrolyte (see **Fig. 7**). The poor stability of N-C@CNT-900 in acidic electrolyte can be attributed to an accepted reason that the existence of large numbers of nitrile N species may accelerate destruction of the N-C@CNT-900 under acidic condition.[36] In addition, above results demonstrated that N-C@CNT-900 had good durability under the alkaline condition, and would be suitable for catalysis of the ORR in alkaline electrolytes.

In recent years, many researches have largely focused on exploration of ORR-active sites in the nitrogen-doped carbon materials, but the function of the real "electrocatalytically active sites" remains unclear because their contribution to the ORR activity is not well-defined. It was proposed by several groups that the improved ORR activity derived from the existence of electron-rich nitrogen functionalities, in particular pyridinic N, pyrrolic N, and graphitic N,[21-23,36,38] which was accounted for by a fact that nitrogen doping in carbon materials will lead to chemically active, localized areas of higher electron density and promotes the catalysis of ORR in aqueous electrolytes.[40,41] These opinions were further supported by theoretical calculation, importantly demonstrating that energy barriers for O_2 dissociation at a carbon atom can be efficiently reduced by the doping of an adjoining nitrogen atom in both carbon nanotubes and graphene, and the decrease in energy barrier is more significant by the graphitic-type nitrogen that other types of nitrogen.[42] Zheng, et al. confirmed that larger amount of graphitic nitrogen species plays an active role in the excellent ORR activity in alkaline electrolyte.[40] Moreover, our previous results also suggested that high content of pyrrolic-type nitrogen incorporating into a carbon matrix may be an effective promoter for ORR, and can play a critical role in the enhancement of the ORR activity of N-doped carbon materials.[26] On the basis of the XPS results and

electrochemical data, we here found that the pyrrolic-type nitrogen species was not contained in the N-C-900 sample, but it could exhibit electrocatalytic activity toward ORR in both alkaline and acidic media. This finding provides strong evidence for a fact that the graphitic-like nitrogen atoms existed in N-C-900 material has played a significant role in maintaining the ORR activity in addition to poor or no activity of oxidized and nitrile N species, and may be the N functionality that is most responsible for the ORR activity and may be the catalytically active site for ORR, which are in good agreement with the previously reported results.[43,44] Meanwhile, it was noted that the occurrence of pyrrolic-like nitrogen species resulted in an obvious increase of the ORR activity of N-C@CNT-900 compared with N-C-900, because the electron-withdrawing effect of pyrrolic-N could activate the adjacent carbon atoms and produce a net positive charge on neighboring carbons, assisting the adsorption and reduction of the O_2 molecule on carbon atoms.[40] Our results indicated that here the pyrrolic nitrogen atoms may be important to enhance the ORR activity only, but may be not the key configuration of catalytic sites. Further researches are in process to test and verify the real function of the active sites, and to predict the correct geometry of N atoms in graphite lattice for the ORR process.

Conclusions

Herein, we developed a facile and cost-effective approach based on pyrolysis at 900 °C to the design of a new nitrogen-doped carbon nanomaterial (N-C@CNT-900) from enoki mushroom, an amino acid-rich, abundantly available, and renewable biomass that acted as a single precursor for both carbon and heteroatoms, therefore avoiding the usage of complicated chemicals in the synthesis processes. The prepared N-C@CNT-900 exhibited more excellent ORR catalytic activity and better durability in alkaline electrolyte than those in acidic electrolyte. More notably, the ORR onset potential measured on N-C@CNT-900 was about 0.94 V in alkaline electrolyte, approaching to that on the state-of-the-art Pt/C catalyst (0.98 V). This may be accounted for by high percentage of graphitic and pyrrolicnitrogens in the N-C@CNT-900 sample. Especially, the graphitic-like nitrogen atoms in the carbon lattice may be the nitrogen functionalities that are the most responsible for the ORR activity and can function as the catalytically active sites for ORR in both alkaline and acidic media. However, the pyrrolic nitrogen can act as an effective promoter for ORR only in this work. It is quite interesting that N-C@CNT-900 can significantly improve the kinetics of the ORR and is also promising for the four-electron O_2 reduction pathway in both alkaline and acidic media. Thus, this study demonstrated that the pyrolysis of enoki mushroom biomass as an only nitrogen precursor at controlled temperatures might be a practicable route to design highly efficient and durable N-doped metal-free catalysts for a range of important electrochemical reactions.

Acknowledgments

This work was financially supported by the Scientific and Technological Research Program of Chongqing Municipal Education Commission (KJ1501118), the Basic and Frontier Research Program of Chongqing Municipality (cstc2014jcyjA50038), the Talent Introduction Project (R2014CJ02) and Scientific Research Project (Y2014CJ24) of Chongqing University of Arts and Sciences. Prof. Zhongbin Li was supported by Graphene Specialized Program of Center for Materials Interdisciplinary Science of Chongqing University of Arts and Sciences. The authors are very grateful to Zhongli Luo, Linhong Jiang, Qinghong Luo, and Jie Huang for helpful discussions.

Notes and references

1 L. Dai, Y. Xue, L. Qu, H.-J. Choi, J.-B. Baek, *Chem. Rev.*, 2015, doi: 10.1021/cr5003563.
2 F. Cheng, J. Chen, *Chem. Soc. Rev.*, 2012, 41, 2172–2192.
3 J. Greeley, I.E.L. Stephens, A.S. Bondarenko, T.P. Johansson, H.A. Hansen, T.F. Jaramillo, J. Rossmeisl, I. Chorkendorff, J.K. Nørskov, *Nat. Chem.*, 2009, 1, 552–556.
4 D. Wang, H.L. Xin, R. Hovden, H. Wang, Y. Yu, D.A. Muller, F.J. DiSalvo, H.D. Abruña, *Nat. Mater.*, 2013, 12, 81–87.
5 G. Wu, P. Zelenay, *Accounts Chem. Res.*, 2013, 46, 1878–1889.
6 W. Ding, L. Li, K. Xiong, Y. Wang, W. Li, Y. Nie, S. Chen, X. Qi, Z. Wei, *J. Am. Chem. Soc.*, 2015, 137, 5414–5420.
7 F. Sedona, M.D. Marino, D. Forrer, A. Vittadini, M. Casarin, A. Cossaro, L. Floreano, A. Verdini, M. Sambi, *Nat. Mater.*, 2012, 11, 970–997.
8 Y. Liang, Y. Li, H. Wang, J. Zhou, J. Wang, T. Regierand, H. Dai, *Nat. Mater.*,2011, 10, 780–786.
9 W.T. Hong, M. Risch, K.A. Stoerzinger, A. Grimaud, J. Suntivich, Y. Shao-Horn, *Energy Environ. Sci.*, 2015, 8, 1404-1427.
10 S. Gao, X. Wei, H. Fan, L. Li, K. Geng, J. Wang, *Nano Energy*, 2015, 13, 518–526.
11 J. Shui, M. Wang, F. Du, L. Dai, *Sci. Adv.*, 2015, 1, e1400129.
12 H. Jin, H. Zhang, H. Zhong, J. Zhang, *Energy Environ. Sci.*, 2011, 4, 3389–3394.
13 S. Wang, D. Yu, L. Dai, D.W. Chang, J.-B. Baek, *ACS Nano*, 2011, 5, 6202–6209.
14 K. Gong, F. Du, Z. Xia, M. Durstock, L. Dai, *Science*, 2009, 323, 760–764.
15 Z. Yang, H. Nie, X. Chen, X. Chen, S. Huang, *J. Power Sources*,2013, 236, 238–249.
16 Z. Mo, S. Liao, Y. Zheng, Z. Fu, *Carbon*, 2012, 50, 2620–2627.
17 C.-Z. Guo, W.-L. Liao, L. Sun, C.-G. Chen, *Int. J. Electrochem. Sci.*, 2015, 10, 2467–2477.
18 Z. Lin, G.H. Waller, Y. Liu, M. Liu, C. Wong. *Nano Energy*, 2013, 2, 241–248.
19 X. Liu, Y. Zhou, W. Zhou, L. Li, S. Huang, S. Chen. *Nanoscale*, 2015, 7, 6136–6142.
20 C.-Z. Guo, W. Liao, C.-G. Chen, *J. Power Sources*, 2014, 269, 841–847.
21 F. Liu, H. Peng, C. You, Z. Fu, P. Huang, H. Song, S. Liao, *Electrochim. Acta*, 2014, 138, 353–359.
22 H. Yang, H. Li, H. Wang, S. Ji, J. Key, R. Wang,*J. Electrochem. Soc.*, 2014, 161, F795–F802.
23 H. Zhao, K. S. Hui, K.N. Hui, *Carbon*, 2014, 76, 1–9.
24 K. Wang, H. Wang, S. Ji, H. Feng, V. Linkov, R. Wan,*RSC*

Adv.,2013, 3, 12039–12042.
25 J. Maruyama, T. Hasegawa, S. Iwasaki, H. Kanda, H. Kishimoto, *ACS Sustainable Chem. Eng.*, 2014, 2, 493−499.
26 C.-Z. Guo, C.-G. Chen, Z.-L. Luo, *J. Power Sources*, 2014, 245, 841–845.
27 C.-Z. Guo, C.-G. Chen, Z.-L. Luo, *Int. J. Electrochem. Sci.*, 2013, 8, 8940–8950.
28 C.Z. Guo, W.L. Liao, C.G. Chen, *Chin. Sci. Bull. (Chin. Ver.)*, 2014, 59, 3424–3429.
29 C. Guo, W. Liao, Z. Li, C. Chen, *Carbon*, 2015, 85, 279–288.
30 Z. Ma, C. Guo, Y. Yin, Y. Zhang, H. Wu, C. Chen, *Electrochim. Acta*, 2015, 160, 357–362.
31 S. Wang, D. Yu, L. Dai, D.W. Chang, J.-B. Baek, *ACS Nano*, 2011, 5, 6202–6209.
32 W. Zhang, P. Sherrell, A.I. Minett, J.M. Razal, J. Chen, *Energy Environ. Sci.*, 2010, 3, 1286–1293.
33 L. Qu, Y. Liu, J.-B. Baek, L.Dai,*ACS Nano*, 2010, 4, 1321–1326.
34 Z. Mo, R. Zheng, H. Peng, H. Liang, S. Liao, *J. Power Sources*, 2014, 245, 801–807.
35 J. Zheng, C. Guo, C. Chen, M. Fan, J. Gong, Y. Zhang, T. Zhao, Y. Sun, X. Xu, M. Li, R. Wang, Z. Luo, C. Chen, *Electrochim. Acta*, 2015, 168, 386–393.
36 W. Ding, Z. Wei, S. Chen, X. Qi, T. Yang, J. Hu, D. Wang, L. Wan, S. Alvi, L. Li, *Angew. Chem. Int. Ed.*, 2013, 52, 11755–11759.
37 Z. Liu, H. Nie, Z. Yang, J. Zhang, Z. Jin, Y. Lu, Z. Xiao, S. Huang, *Nanoscale*, 2013, 5, 3283–3288.
38 H. Peng, F. Liu, X. Liu, S. Liao, C. You, X. Tian, H. Nan, F. Luo, H. Song, Z. Fu, P. Huang, *ACS Catal.*, 2014, 4, 3797−3805
39 X. Fu, Y. Liu, X. Cao, J. Jin, Q. Liu, J. Zhang, *Appl. Catal. B*, 2013, 130-131, 143–151.
40 B. Zheng, J. Wang, F.B. Wang, X.H. Xia, *Electrochem. Commun.*, 2013, 28 , 24–26.
41 H. Niwa, K. Horiba, Y. Harada, M. Oshima, T. Ikeda, K. Terakura, J. Ozaki, S. Miyata, *J. Power Sources*, 2009, 187, 93–97.
42 Y. Shao, J. Sui, G. Yin, Y. Gao, Appl. Catal. B, 2008, 79, 89–99.
43 H. Niwa, K. Horiba, Y. Harada, M. Oshima, T. Ikeda, K. Terakura, J. Ozaki, S. Miyata, *J. Power Sources*, 2009, 187, 93–97.
44 T.C. Nagaiah, S. Kundu, M. Bron, M. Muhler, W. Schuhmann, *Electrochem. Commun.*, 2010, 12, 338–341.